Radio Interferometric Determination of Source Positions, Intercontinental Baselines, and Earth Orientation With Deep Space Network Antennas – 1971 to 1980

J. B. Thomas, O. J. Sovers, J. L. Fanselow,
E. J. Cohen, G. H. Purcell, Jr., D. H. Rogstad,
L. J. Skjerve and D. J. Spitzmesser
Tracking Systems and Applications Section

A series of experiments has been conducted at the Jet Propulsion Laboratory during the last decade to develop a radio interferometric system capable of measuring crustal and rotational motions of the earth, as well as source positions for a reference frame based on compact extragalactic radio sources. With the exception of one session between Big Pine, Calif., and Westford, Mass., the observing stations were those of NASA's Deep Space Network in California, Spain, and Australia.

Approximately 2400 observations of extragalactic radio sources were made between August 1971 and February 1980 during 48 separate sessions. These consisted of 259 delay rate observations at 2.3 GHz (S-band), 796 delay and delay rate observations at either S-band or 8.3 GHz (X-band) and 1325 delay and delay rate observations recorded simultaneously at both S- and X-band. A single multiparameter fit has been applied to the observed values of delay and delay rate to extract astrometric and geophysical parameters from this decade-long sequence. The fit produced estimates of 784 parameters, including station locations, radio source positions, polar motion, Universal Time, the precession constant, and solid earth tides. The a priori model included gravitational bending, the 1980 IAU nutation series, the 1976 IAU expressions for Greenwich mean sidereal time and precession, BIH estimates of Universal Time and polar motion, and monthly mean values for zenith troposphere delay.

The rms residuals were 0.52 nsec for delay and 0.30 psec/sec for delay rate. Intercontinental baseline lengths have been determined with formal uncertainties of 5 to 10 cm. Universal Time and polar motion were measured at 49 epochs, with formal uncertainties (for the more recent data) of 0.5 msec for UT1 and 6 and 2 mas, respectively, for the X and Y components of polar motion. Our 1971–80 data produced a formal estimate of the luni-solar precession constant that was smaller than the 1976 IAU value by –3.8 ±

0.9 mas/year. However, due to the relatively short span of data and the inaccuracy of the earlier data, the precession effect could not be separated from the effect of the 18.6-year nutation term. Further, the less reliable data in the earlier years may have biased our precession result by an amount considerably larger than the formal error of 0.9 mas/year. The result for the gamma factor of the parameterized post-Newtonian formalism was 0.997 ± 0.041, which agrees very well with general relativity. The vertical and horizontal Love numbers have been determined with 5% and 30% uncertainties, respectively, while the earth tide phase lag was found to be zero within its error estimate. These earth-tide results agree with the commonly accepted values. In addition to these geophysical results, the positions of 104 sources have been obtained with formal uncertainties of approximately 5 milliarcseconds.

I. Introduction

Over the last few years, considerable progress (Refs. 1–5) has been made toward realizing the potential of radio interferometry for measuring local crustal and global rotational motions of the earth with accuracies at the centimeter level. Toward this goal, a series of experiments, primarily with NASA's Deep Space Network (DSN) antennas, has been conducted over the last decade to develop two generations of very long baseline interferometric (VLBI) systems. In all, 48 interferometric sessions were carried out between eight different antennas on three continents. Delay and/or delay rate observables were measured on two local baselines (at Goldstone, California, and at Madrid, Spain), on a transcontinental baseline (Big Pine, California to Westford, Massachusetts) and two intercontinental baselines (Goldstone, California to Madrid, Spain, and Goldstone, California to Tidbinbilla, Australia). A single multiparameter fit has been applied to this decade-long sequence of observations to extract significant astrometric and geophysical parameters. The adjusted parameters included station locations, source positions, polar motion, Universal Time, the precession constant, solid earth tides, and the gamma factor of relativity theory. This report outlines the techniques, analyses and results of these experiments.

II. Interferometry Technique

In interferometry measurements, the random broadband emission of an extragalactic radio source is simultaneously recorded at two widely separated radio antennas. Cross correlation of the recorded data at a central site leads to a determination of the difference in arrival times of the radio wavefront at the two antennas. Since this difference (delay) depends on the direction of the source and the vector separation of the antennas, it contains information concerning the rotational and crustal motions of the earth. To extract this information, it is necessary to measure the delay for many different sources, preferably on several baselines, and to pass the resulting delays through a multiparameter fitting program that solves for astrometric and geophysical quantities.

In the present experiments, two separate interferometry systems have been used to measure delay and delay rate. Since the instrumentation and data processing techniques have been described elsewhere (Refs. 6, 7), we will only summarize the most salient features of the two systems. The prototype system used in the early measurements recorded a single, narrowband (24-kHz) channel at S-band (2.3 GHz) and therefore could measure only delay rate accurately. Since the delay rate observable is independent of the polar component of the baseline vector and is less powerful in parameter estimation than delay, another system was developed to measure both delay and delay rate. This system records several time-multiplexed frequency channels so that delay can be obtained by means of bandwidth synthesis, a technique pioneered by Rogers (Ref. 8). The bandwidth of the individual channels was also increased to 2 MHz to improve flux sensitivity and signal-to-noise ratio. Bandwidth limitations at the first stage of amplification in the Deep Space Network receiver systems limited the maximum bandwidth spanned by the outer channels in a given radio frequency (RF) band to about 40 MHz. With this bandwidth synthesis system, delay could be measured with a precision (i.e., system noise error) of approximately 100 psec, given a typical source strength of 0.5 Jy, an integration time of 3 min, and two 64-m DSN antennas with system temperatures of 35 K. By cycling through two sets of channels properly placed at RF, the second system was capable of "simultaneously" measuring delay at S-band and X-band (8.4 GHz).

III. Geometric Delay Model

The delay (or delay rate) observable measured by radio interferometry is a sum of the differential delays (or rates) due to geometric, instrumental, ionospheric, and tropospheric effects. This section summarizes a mathematical model for the geometric delay that was developed by Fanselow (Ref. 9).

The geometric delay, which is by far the largest (up to 30 msec) of the delay terms, is of primary interest in the current measurements since it depends on the direction of the incom-

ing wave and on the time-varying baseline vector between antennas. Consequently, a calculation of the geometric delay must include, in addition to the radio source location, all significant factors describing the rotational, crustal, and orbital motions of the earth.

Models of the geometric delay usually place the origin of coordinates at either of two points: the center of mass of the earth (geocentric approach) or the center of mass of the solar system (solar-system-barycentric approach). Even though the approximate delay model generated by the geocentric approach is mathematically simpler in its final form, the solar-system-barycentric (SSB) approach is inherently more adaptable to refinements in the geometric delay model, particularly for relativistic effects. Consequently, even though such refinements are not justified by the limited accuracy of the present data, the SSB approach has been adopted in anticipation of model improvements that will be demanded by future, more accurate data. In other applications, the SSB approach would facilitate generalization to accommodate sources (such as spacecraft) within the solar system.

A geometric delay model that adequately describes the present data can be based on the following theoretical assumptions. Given a set of SSB coordinates defined in terms of the mean equator of J2000.0, suppose that a wavefront with propagation direction $\hat{\mathbf{k}}$ is received by two earth-fixed antennas whose time-varying positions in SSB coordinates are given by $\mathbf{x}_1(t)$ and $\mathbf{x}_2(t)$ at TDB (barycentric dynamical) time t. In terms of these quantities, the geometric delay between antennas will be given approximately by

$$\tau_g(t) = \frac{\hat{\mathbf{k}} \cdot [\mathbf{x}_2(t) - \mathbf{x}_1(t)]}{1 + \dfrac{\hat{\mathbf{k}} \cdot \mathbf{v}_2(t)}{c}} \qquad (1)$$

where the dot product involving $\mathbf{v}_2$ (the velocity of antenna 2) accounts for motion of antenna 2 during the wave transit. Since the measured delay is obtained by earth-fixed observers, the theoretical delay in Eq. (1) must be relativistically transformed to earth-fixed coordinates. For the present data, this transformation is adequately applied with a special relativistic (Lorentz) transformation that introduces, as its largest effect, the equivalent of the well-known "earth-centered" aberration correction to the source location. General relativistic effects, except for gravitational bending of radio waves, are neglected. A correction term is applied to the SSB model delay to account for such gravitational bending prior to transforming back to an earth-centered coordinate system.

To obtain the SSB antenna "trajectories" $\mathbf{x}_i(t)$ used in the above delay calculation, a model for the rotational and orbital motions of the earth must be adopted. Our present rotational model for the earth is the model summarized by Kaplan (Ref. 10), including the earth's spin axis direction from the IAU 1976 precession (Ref. 11) and the IAU 1980 expressions for nutation (Refs. 12, 13) and Greenwich mean sidereal time (Ref. 14). Orientation about the spin axis, parameterized as Universal Time (UT1), is treated as a solve-for parameter, as is polar motion (the position of the ephemeris pole with respect to the earth's crust). Station locations are defined relative to an earth-fixed frame with its Z axis along the mean spin axis of 1903.0 and X axis along the Greenwich meridian. Within this frame, generally referred to as the CIO (Conventional International Origin) frame, the station locations are expressed in terms of cylindrical coordinates. Axis orientation for the earth-fixed CIO frame is experimentally determined through the use of Universal Time and polar motion (UT/PM) values measured by the Bureau International de l'Heure (BIH), as explained in Sec. VII. Since all these conventional earth orientation parameters are defined relative to geocentric coordinates, the final step in the calculation of the SSB antenna positions $\mathbf{x}_i(t)$ involves a special relativistic transformation of the positions from geocentric coordinates to SSB coordinates. The earth's orbital motion is obtained from numerically integrated ephemerides developed at the Jet Propulsion Laboratory (Ref. 15).

IV. Propagation Media Calibrations

The total measured delay is corrupted by differential delays due to the propagation media traversed by the radio waves. This section outlines the calibration techniques used to correct for the delays introduced by the troposphere and charged particles.

Due mainly to changes in slant range, the delay produced by the troposphere varies as a function of antenna elevation angle. At a 10-deg elevation angle, the tropospheric delay is approximately 40 nsec (12 m) while, in the local vertical (zenith) direction, it is approximately 7 nsec (2 m). For the present data, a priori corrections for these atmospheric delays were derived from a monthly-mean troposphere model developed at JPL (Chao, Ref. 16) to calibrate radiometric data for spacecraft navigation. For each month of the year, Chao obtained from regional meteorological data mean values for the zenith delays due to the wet and dry components of the troposphere. The tropospheric delay for a given antenna pointing direction can be calculated by mapping the appropriate monthly-mean total zenith delay (dry plus wet) according to an elevation-dependent mapping equation derived from a ray-trace analysis (Ref. 16). Chao estimates the accuracy (1σ) of this calibration technique to be about 3% of the applied correction, or about 40 cm in the worst case. Since the overall uncertainties (1σ) in the delays measured in the later experiments were approximately 15–30 cm, a priori errors in the

tropospheric delays were about the same as the sum of the combined effects of the other observable errors. For this reason, zenith tropospheric delays were also estimated in the multiparameter fit (Sec. VII), but were constrained to the Chao model at the 3% level by means of an additive covariance constraint matrix.

The ionospheric contribution to the observed delays falls approximately in the range 4–50 cm at X-band, depending on antenna elevation and the electron content of the ionosphere. Ionosphere calibrations were handled in two different ways. In later experiments, both S-band and X-band delays were generally measured so that dual-band calibrations were possible. In principle, the ionospheric effect and any other space plasma effect were thereby reduced to a level below other errors in the delay observables in those particular sessions. Ionospheric delays in the single-band sessions were corrected through the use of satellite-Faraday-rotation data. The corrections were obtained by mapping a reference 24-hour zenith delay signature to the time, longitude and, direction of each observation. The reference signature was obtained by averaging the daily Faraday-rotation measurements gathered over a period of 3 months (July–Sept.) in 1971 at Sagamore Hill, Mass. (Ref. 17). It is estimated that this calibration procedure reduces the ionospheric effect by approximately 65%, so that the worst-case observable error due to the ionosphere is roughly 20 cm at X-band. This mean-signature approach to ionosphere calibration was adopted for the single-band experiments due to the unavailability of reliable Faraday-rotation data at the desired times and locations.

V. Observing Strategy

In order to measure both polar motion and Universal Time at a given epoch, concurrent or nearly concurrent measurements on two nonparallel baselines, ideally orthogonal, are required. This requirement is a consequence of the fact that the delay and delay rate observables for a given baseline are insensitive to earth rotations about that baseline vector. In the present experiments, the California/Spain baseline, which is essentially east-west, is sensitive to UT1 and to the X component of polar motion but is relatively insensitive to the Y component of polar motion. In contrast, the California/Australia baseline is sensitive to UT1 and to the Y component of polar motion but is much less sensitive to the X component. Thus, the combination of nearly concurrent observations on both these baselines can yield accurate measurements of all three rotational parameters.

The sources observed on a given day were chosen to cover the full range of directions allowed by the mutual visibility of the two stations. A wide range of source directions is desirable to "separate" sensitivity partial derivatives in the multiparameter fit and thereby to reduce errors in estimated parameters, as well as correlations among the errors. During each observing session, an attempt was made to observe each source at least three times in such a way that the observations completely spanned the interval of mutual visibility between stations for each source. The cycling sequence through the allowed observing directions also was made as random as possible in order to reduce correlations with possible periodic errors in the observables.

To strengthen the overall solution, the source lists for separate sessions were often made identical, particularly when additional measurements could still significantly improve the errors in given source locations. Repetitive observations of the same sources also provide an opportunity for consistency checks, namely whether different subsets of the data yield the same location for a given source or for a given antenna within experimental error. Another requirement affecting source selection was that both intercontinental baselines (California/Spain and California/Australia) observe largely the same sources between −10 and +40 deg declination, the region of the celestial sphere that is mutually visible. The presence of a wide range of sources common to both baselines greatly reduces correlations between parameters, such as the strong correlations found in single-baseline solutions for the California/Australia baseline with its limited mutual visibility. Such a strategy can also remove the near-singularity in declination associated with zero-declination sources in single-baseline solutions with the nearly east-west California/Spain baseline.

VI. Summary of Experiments

Over the last ten years, 48 interferometry sessions have been carried out with eight observing antennas. The diameter and approximate efficiency and zenith system temperature for each of these antennas are presented in Table 1. The first five antennas are DSN facilities; the antenna at Big Pine, Calif., is at the Caltech Owens Valley Radio Observatory, and the Westford, Mass., antenna is at the Haystack Observatory. For each session, Table 2 gives the date, antenna pair, session length, number of sources, number of observations, observable type (delay and/or delay rate), observing frequency, and types of station frequency standard. All together, there were 2382 observations of 117 sources taken during 23 S-band sessions, 5 X-band sessions and 20 dual-band sessions. Depending on the session, the station frequency standards were rubidium, cesium or hydrogen masers.

For each source, Table 3 gives the number of sessions in which that source was observed, the average epoch of observation, and the number of observations of delay and delay rate. Three fourths of the 117 sources are observed at least 20 times, with a high of 161 observations for 4C 39.25. Average observa-

tion epochs (calculated by weighting all observations equally) range from 1976.36 for NRAO 190 to 1980.15 for GC 1128+38.

VII. Fitting Technique

After the observations had been reduced to delay and/or delay rate, the resulting observables were passed to a multiparameter weighted-least-squares program that simultaneously fit all of the delay and delay rate data to obtain estimates of geophysical and astrometric parameters (Ref. 9). Solve-for parameters in the fit could be grouped into two categories. The first category involved parameters specific to a given observing session and included clock rate and epoch, polar motion, Universal Time (UT1) and troposphere parameters for each station. The second category involved "global" parameters common to more than one session and included station locations, two position angles per source, solid-earth-tide parameters, the gamma factor of general relativity and the precession constant. When necessary for any given parameter, the data were organized into segments, over each of which an independent value could be estimated for that parameter in the grand fit to all of the data. For example, this capability was employed for clock parameters, for which it was quite often necessary to divide a session into a number of parts, in each of which a linear or quadratic function of time was applied. To parameterize the troposphere model, the longer sessions were divided into 12-hour portions at each station, each with an independent zenith troposphere delay. Finally, in special tests for repeatability of source-position and station-location parameters, similar divisions were made.

In an ideal measurement of UT/PM with DSN stations, concurrent sessions would be carried out on the California/Spain and California/Australia baselines. Since concurrent sessions are not possible due to constraints of mutual visibility, nearly concurrent sessions on adjacent days were scheduled whenever possible. In this imperfect approach, UT1, which is fairly rapidly varying, was modeled as an independent parameter in each session. On the other hand, more slowly varying polar motion was modeled as a single pole position for the two adjacent sessions. Thus when UT/PM results are presented for adjacent sessions, only a UT1 value will be listed for each session, while PM values will be listed for a fictitious session at the mean time of the two sessions.

The observables in the fit were weighted in inverse proportion to the square of a total error computed as the root-sum-square of the estimated errors from known error sources. The two estimated delay errors were system noise (100 to 545 psec) and ionosphere error for single-band data (35% of ionosphere delay, which equalled 2 to 18 cm for X-band). An explicit troposphere error was not included in the observable weighting since the troposphere was accounted for (to first approximation) through the covariance matrix in the form of a solve-for parameter. In addition to these individually estimated errors, an adjustable session-specific error was root-sum-squared with the other errors in order to account for unestimated or underestimated errors in the data. To estimate the adjustable error, several preliminary fits were made in which this error was adjusted until the normalized chi-square computed separately for the delay and delay rate observables was approximately equal to 1.0 for each session and for the overall fit. Although this treatment of observable noise is far from perfect, it does provide, to a first approximation, an estimate of total observable noise that is based both on a priori information and on the fit residuals.

Two problems encountered in VLBI multiparameter fits are specification of the origin of right ascension and the establishment of an earth-fixed coordinate frame. In this work we have adopted for the right ascension of 3C 273B the value $12^h\ 29^m\ 6\overset{s}{.}6997$ in order to match the definition currently used by many VLBI observing groups. We view this approach as a temporary convenience until it is possible to align our reference frame with the celestial reference frame defined by the JPL planetary ephemeris. To obtain that alignment, the Astronomical Measurements Group at JPL is currently analyzing data from a number of radio interferometry experiments designed to measure the difference in the delay obtained for a spacecraft in orbit about a planet and the delay obtained for a nearby extragalactic source.

For alignment of the axes of the earth-fixed frame with the CIO frame, a two-step procedure based on an a priori covariance matrix is more accurate than the usual approach of relying on BIH values for UT/PM on a single selected reference day. The first step is a fit in which all UT/PM parameters are allowed to vary within the constraints imposed by the BIH values and their errors. This step implicitly minimizes, over the span of the observations, the rms deviation of interferometrically measured UT1 and polar motion from BIH a priori values. In subsequent fits, the UT/PM solve-for values obtained in the first step for two strong adjacent sessions (reference days) are assigned as exactly known quantities. With this approach, subsequent UT/PM values and the axes of the earth-fixed frame are aligned on average with the conventional definitions in the best way provided by the data in hand. For the present data, we estimate that the resulting alignment with BIH conventions is accurate to 2–5 mas for the polar axis and to 0.4–1.0 msec for longitude.

Since interferometry observables for extragalactic sources are insensitive to the origin of the earth-fixed frame, data content by itself does not require the consideration of that

origin. However, for computational reasons, it is desirable to use station locations as the solve-for parameters rather than baseline vectors. With this approach, at least one station (the reference station) must be assigned an a priori position to establish the origin of the earth-fixed frame and thereby prevent singularity in the least-squares solution. Thus, in addition to the axis orientation error mentioned above, the adjusted locations of the other stations are subject to errors that are a consequence of errors in the a priori location of the reference station.

For the present data, the choice of a reference station is relatively simple. Of the eight stations at which the observations were made (see Table 1), all but two are linked to the deep space station (DSS 14) at Goldstone, Calif., either by direct two-station observations or through a common third station. The two exceptions are the Owens Valley (OVRO) and Westford, Mass. (HAYST) antennas, for which a disjoint 48-hour session comprises the only data. To avoid defining a second reference station, the location of OVRO was linked to DSS 13 at Goldstone by employing DSS 13–OVRO baseline measurements made by the ARIES project (Ref. 18). In our fits, each component of this baseline was constrained to equal the ARIES result on the basis of the ARIES formal uncertainties (~9 cm). The only other sessions not involving station DSS 14 (DSS 11–DSS 43 on 77/2/1 and DSS 62–DSS 63 on 79/11/15) have both stations participating in direct observations with DSS 14 on other dates. Thus, with the addition of this constraint on the DSS 13–OVRO baseline, all seven station locations could be referenced to an assigned value for the DSS 14 location. For this assigned value, we chose the coordinates from station location set LS111A derived from spacecraft tracking (Ref. 19). Moyer estimates the DSS 14 location error to be ~1 m in spin radius, ~2–5 m in longitude, and ~10 m in Z-height. As mentioned above, these reference station errors will lead to a systematic bias in all station positions. On the other hand, the relative locations of the stations have uncertainties that are determined by the quality of the VLBI observations, the accuracy of the delay model, and the size of the alignment errors for the earth-fixed axes.

VIII. Results

The majority of the results presented in this section were derived from a single "standard" fit to the 1971–80 delay and delay-rate observables in which parameters were adjusted for source positions, station locations and clocks, UT/PM, tropospheric delays, gravitational bending and solid earth tides. In addition to the features discussed in Sec. VII, astronomical constants, time scales and the fundamental reference frame were in accord with the IAU resolutions to be implemented to 1984 (as summarized by Kaplan (Ref. 10)).

For an overall view of the goodness of fit, Table 4 shows for each session the rms residual delay and delay rate obtained with the standard fit. While the overall averages are 0.52 nsec and 0.30 psec/sec, variation among sessions is considerable, with the best sessions giving substantially smaller residuals.

To assess the contribution of the delay rate observables to the adjusted parameters and their estimated uncertainties, another fit was performed. This was identical to the standard fit, except that only the delay observables were used, and thus only sessions after 77/1/12 were included (see Table 2). The resulting parameter values were consistent with those from the standard fit. Typically, formal uncertainties from the standard fit were smaller than those from the delay-only fit by 30% for station coordinates, 20% for source positions, and 15% for Universal Time and polar motion. Numerous fits were necessary to determine the magnitudes of the adjustable observable errors (see Sec. VII) that corresponded to chi-square values of 1.0. These fits indicated that all solve-for parameters were fairly insensitive to the values of the adjustable errors. For example, any given solve-for parameter varied by a small fraction of its formal uncertainty when the adjustable errors were varied over a range corresponding to chi-square between 0.9 and 1.1. Additional special fits to the data have been performed for specific purposes such as source-position and baseline repeatability tests and adjustment of nutation and precession, as discussed below.

A. Source Positions

The last columns of Table 3 give, in terms of right ascension and declination, the J2000.0 positions of 117 sources resulting from the standard fit to the 1971–80 VLBI data. Of these, seven (3C 48, 3C 119, 3C 138, 3C 309.1, 3C 395, 3C 418 and DA 611) were observed only on short baselines, and thus have formal position errors exceeding 0.″1. One source (4C 55.16) was observed only once on an intercontinental baseline and its position must therefore be used with caution. Another, low-declination source (P 1130 + 009) was not observed on the California/Australia baseline and therefore has a large declination error. Other sources for which there are fewer than 5 delay observations may also lack adequate redundancy. All listed errors are 1σ formal uncertainties obtained from the covariance matrix of the standard fit and thus do not properly account for errors due to mismodeling of precession and nutation.

The statistics of our source catalog are more clearly demonstrated in Figs. 1–3. Figure 1 presents the source distribution in terms of right ascension and declination, with error bars indicating formal uncertainties. (Note the different scales for position and uncertainty.) In Figs. 2 and 3, histograms of the arc length errors for RA and declination indicate that the

mean position error is approximately 5 mas for both coordinates.

In order to determine the repeatability of source positions over a long period of time, and to test the validity of the formal error estimates, the data were divided into two segments: observations made before January 1979 and observations made after May 1979. The average measurement epochs in these two segments were approximately 1977.5 and 1979.9. All sources with more than 10 (delay + delay rate) observations in each segment were assigned independent position parameters in the two segments. A fit was performed in which all other parameters were solved for as in the standard fit. In Table 5, columns 4 and 5 show the RA and declination differences for the two position estimates, columns 6 and 7 give the root-sum-squared errors, and the last two columns give the differences normalized by the rss errors. The rms differences for right ascension and declination (2.9 and 4.0 mas) are somewhat smaller than the average formal uncertainties for the catalog of Table 3. Figure 4 shows a plot of the position differences in columns 4 and 5 of Table 5. Since Table 5 shows that no normalized difference exceeds 1.6σ, the positions produced by the two segments of data are in very good agreement at the level of the formal uncertainties. Overall, the results indicate that our formal source position errors are close to or perhaps slightly larger than the true random errors. Preliminary comparison with the source catalog of another VLBI group (Refs. 20, 21) resulted in fair agreement but indicated that about a 50% increase in formal uncertainties might be needed.

B. Station Locations and Baselines

Table 6 presents the station locations obtained from the standard fit to the entire data span. As discussed in Sec. VII, station DSS 14 at Goldstone is the reference station, and the other seven locations are adjusted. The value 299792.458 km/sec was used for the velocity of light. Formal error estimates of the station coordinates range from ~2 cm for DSS 13 to ~56 cm for the poorly determined equatorial component of DSS 11. The formal uncertainties for the station locations are relative errors and do not account for the uncertainties from orienting the axes of the earth-fixed frame or from the assignment of the DSS 14 location.

Rather than present all 28 baselines between the eight stations, we focus attention on the six typical station pairs given in Table 7, which include two intercontinental (DSS 14 to DSS 43 and DSS 63), one transcontinental (OVRO to HAYST), and three local (DSS 14 to DSS 11 and DSS 13, DSS 62 to DSS 63) baselines. Anomalously high formal errors for the DSS 14–DSS 11 baseline are due to the fact that no direct DSS 14–DSS 11 observations were included in the fit. Since baseline errors, unlike baseline vectors, cannot be computed accurately from Table 7, formal uncertainties of components and lengths of all 28 baselines are listed in Table 8. These formal uncertainties do not account for the errors in orienting the axes of the earth-fixed frame.

Two comparisons of baseline lengths with results of independent investigations are possible. For the OVRO-HAYST baseline, the east coast VLBI group (Ref. 22) obtained a length of 3928881.59 ± 0.02 m based on data extending from July to October 1980. This result is in excellent agreement with our length measurement. A 1975 ground survey of the DSS 62–DSS 63 baseline (Ref. 23) gives a length of 10452.61 m, also in excellent agreement with our result.

To test for baseline length repeatability, another special fit to all the data was performed in which independent station location parameters were assigned to DSS 43 and DSS 63 for each relevant post–1976 intercontinental session of Table 2. This led to 20 estimated values for the Australian station (DSS 43) and 12 for the Spanish station (DSS 63), with both spanning a 3-year period. The Goldstone station (DSS 14) was assigned the same common reference location (see Table 6). To avoid a singular solution, the UT/PM parameters were held fixed at the results of the standard fit. All other parameters were treated as in the standard fit. The baseline length results from this fit, which are shown in Figs. 5 and 6 along with 1σ formal uncertainties, exhibit several interesting features. First, we note the general decrease of the error estimates with time, which indicates continuing improvement in system performance. Second, comparison of X-band and S/X results with S-band results indicates that the S-band baselines were corrupted by as much as 100 cm by ionospheric effects for both baselines. Third, even though there may be a suggestion of change, there is no convincing evidence of relative motion between stations. To quantitatively assess possible changes in baseline lengths over the years, however, a linear function of time has been separately fit to the length results for each of these two intercontinental baselines. Due to ionospheric corruption, only the X-band and dual-band results were included in these fits, which led to slopes of −5 ± 5 and +7 ± 10 cm/yr for the baselines to Australia and Spain, respectively. It is of interest to note that, even though these results are consistent with no motion over the 3-year period, both slopes are closer to the length changes inferred (Ref. 24) from a global model (Ref. 25) of plate motion over geological time scales than they are to the assumption of no motion. Morabito's application of the Minster-Jordan model indicates length changes of approximately −4 and +2.5 cm/yr for the baselines to Australia and Spain, respectively. Doppler satellite tracking (Ref. 26) has recently produced measurements of plate motion which appear to be consistent with our baseline results.

C. Polar Motion and UT1

Table 9 presents all the UT/PM values obtained from the standard fit, while Figs. 7 and 8 compare our X and Y polar motion results for 1977–80 with BIH Circular D (Ref. 27). Our UT/PM uncertainties are relative errors and do not include errors resulting from orienting the axes of the earth-fixed frame. If the BIH PM values are assigned an uncertainty of approximately 0.″01, there are no outstanding discrepancies between the two techniques. For the UT1 results similarly plotted in Fig. 9, short-period tidal fluctuations have been removed from the VLBI data in order to permit comparison with the heavily smoothed BIH values. The solid curve represents lunar laser ranging (LLR) data as smoothed over a 10-day interval by Fliegel et al. (Ref. 28) with the same tidal dependence removed. These lunar data originally consisted of several hundred points in the range of the plot. The LLR curve has been displaced vertically in order to remove a 1.0-msec bias between VLBI and LLR values. The figure shows that the UT1 values measured by VLBI, LLR, and BIH generally agree with one another if the BIH values are assigned errors of approximately 2 msec, and the LLR values errors of 1 msec or less. Both the VLBI and LLR results suggest the same oscillation of ~2 msec amplitude about the BIH values. Recent work by Capitaine and Feissel (Ref. 29) indicates that introduction of the 1980 IAU nutation model into the BIH solution results in corrections to UT1-UTC as large as 2 msec. We plan to investigate the impact of such a correction on the above comparison of UT1 results. Two of the three points of large discrepancy (~2 to 3σ) between VLBI and LLR (in February 1980) occurred at the center of a 20-day gap in the LLR data. Thus these differences may represent a real short-period excursion that was not sampled in the LLR measurements. The third point of large discrepancy in February 1977 remains unexplained.

D. Global Parameters

In addition to the source positions and station locations discussed above, global parameters include the precession constant, earth-tide parameters, and the gamma factor of general relativity. The long time span of the data provided an opportunity to solve for the precession constant. Specifically, if we solve for a residual precession rate of the earth, we find that the best fit to our data does not occur for the 1976 IAU precession constant, but for a value smaller than that value by 3.8 ± 0.9 mas/yr (for luni-solar precession). However, this result must be qualified by the observation that the first 6.5 years of our 8.5-yr data span consisted of less reliable data (S-band delay rate only and S-band delay and delay rate data) which may have biased our solution. Since our data cover a time interval small compared to the 18.6-year nutation period, there is a high degree of correlation between the precession constant and the nutation amplitude with that period. Thus our present data cannot accurately separate these two effects. Such a separation will become possible, however, as the span of data approaches a significant fraction of the 18.6-year period. Similar explorations of modified nutation and precession by the JPL group analyzing lunar laser ranging (Ref. 30) have yielded estimates of 8 ± 8 mas/yr for the 18.6-yr nutation term correction, and –2 ± 4 mas/yr for the precession correction.

Since the data were inadequate for determination of independent earth-tide parameters at each station, a universal set of parameters was specified for all stations. This model allowed adjustment of three parameters: the vertical and horizontal Love numbers and the tide phase lag. The standard fit yielded values of 0.63 ± 0.03 and 0.058 ± 0.016 for the vertical and horizontal Love numbers, and 0.0 deg ± 1.5 deg for the tide phase lag. These results are in good agreement with the commonly accepted values of 0.603–0.611, 0.0832–0.0842 and 0 deg (Refs. 31, 32).

Since gravitational deflection of the incoming signal by the sun is a relatively large effect for these long baselines even at large sun-earth-source angles, it is possible to solve for the gamma factor of the parameterized post-Newtonian formalism. The result of 0.997 ± 0.041 is in good agreement with general relativity (Ref. 33).

E. Troposphere Parameters

The dry troposphere parameters obtained from the standard fit are presented in Table 10 along with 1σ formal error estimates. As discussed in Sec. IV, the tropospheric delays for the DSN stations were constrained to the Chao model on the basis of the estimated error (3%) in that model. For sessions involving delay observations (1977–80), the formal uncertainties from our fit are considerably better than the Chao a priori errors. In addition to the standard fit, which was based on 12-hour subdivisions of tropospheric delays, another fit was made in which new troposphere parameters were introduced at each station at 6 a.m. and 6 p.m. local time, in order to investigate the effect of dividing tropospheric delays into day and night portions. No significant effects on any of the adjusted parameters were observed in this fit. The possibility of mismodeling the tropospheric delays at low elevation angles was also considered. A fit that omitted any observation with an elevation angle less than 10 deg at either station produced parameters that differed from those given by the standard fit by no more than the formal uncertainties. Attempts to find correlations between the delays in Table 10 and local atmospheric measurements (when available) were unsuccessful.

F. Clock Parameters

As shown in Table 11, 170 station clock parameters were adjusted in the standard fit to describe clock epoch and rate

offsets and nonlinearities in the delay data. The reference clock is that at DSS 14, with three exceptions. In the two three-station experiments in February 1977, it was necessary to use one of the other station clocks (DSS 11 or DSS 43) as a reference, because of missing data at DSS 14. For the OVRO-HAYST observations in February 1978, the Haystack clock served as a reference. A quadratic clock model was used in only three sessions, while piecewise linear fits were required in 23 of the 48 sessions. For the best sessions, the offsets between station clocks were measured with formal uncertainties of the order of 0.01 psec/sec for clock rate and 0.5 nsec for clock epoch. Since instrumental phase calibration was not employed, the "solve-for" clock parameters are not purely clock offsets, but also include instrumental terms. Thus these accuracies are merely indicative of the capability of this technique once proper instrument calibration is performed. The 73 clock parameters adjusted for the delay rate observables are not reported here.

IX. Discussion and Conclusions

The development of two radio interferometry systems at JPL during the past decade has led to a number of significant astrometric and geophysical results. With the present system, we have measured the lengths of two DSN baselines (California/Australia and California/Spain) with formal uncertainties of 10 cm and 4 cm, respectively. When the baselines were adjusted independently for each observing session, no convincing evidence of change in the length of either baseline was detected. We are continuing to improve the system and accumulate data. If actual rates of tectonic displacement are of the order of 5 cm/yr, we expect to detect them within a few years.

A radio source reference frame has been established which contains 104 sources with positional uncertainties of approximately 5 mas. Our estimates for parameters describing earth tides and gravitational bending agree with commonly accepted values. Further, formal uncertainties in adjusted "clock" parameters indicate a potential for synchronizing station clocks at the nanosecond level.

Our measurements of polar motion and UT1-UTC with formal uncertainties of 5 to 20 cm agreed fairly well with results obtained by the BIH and lunar laser ranging. A fit to our current data produced an estimate for the luni-solar precession constant which is smaller than the IAU value by 3.8 ± 0.9 mas/yr. Because our earlier data are less reliable, more observations are required to verify this result. Since the discrepancy of 3.8 mas/yr is substantially larger than the estimated uncertainty in the IAU value (1 or 2 mas/yr), there is strong motivation to improve the reliability of this result through more measurements.

The results of these observations underscore the importance of improving the scope and accuracy of radio interferometry measurements in a number of areas.

Acknowledgments

J. G. Williams and P. F. MacDoran made pioneering contributions to the radio interferometry program at JPL. We thank the many staff members at the DSS 11, 13, 14, 43, 62, 63, OVRO, and Haystack antennas for their expert attention to instrumentation at the observing stations. A. Rius planned and executed the DSS 62–DSS 63 experiment in November 1979. Finally, we thank J. D. Gunckel for her many hours of dedication in seeing the data through the initial stages of processing.

References

1. Thomas, J. B., et al., "A Demonstration of an Independent-Station Radio Interferometry System with 4-cm Precision on a 16-km Baseline," *J. Geophys. Res.*, 81, pp. 995–1005, 1976.

2. Rogers, A. E. E., et al., "Geodesy by Radio Interferometry: Determination of a 1.24-km Base Line Vector With ~5-mm Repeatability," *J. Geophys. Res.*, 83, pp. 325–334, 1978.

3. Ryan, J. W., et al., "Precision Surveying Using Radio Interferometry," *J. Surveying and Mapping Div., Proc. ASCE*, Vol. 104, No. SU1, pp. 25-34, 1978.

4. Niell, A. E., et al., "Comparison of a Radio Interferometric Differential Baseline Measurement With Conventional Geodesy," *Tectonophysics*, 52, pp. 49–58, 1979.

5. Herring, T. A., et al., "Geodesy by Radio Interferometry: Intercontinental Distance Determinations with Subdecimeter Precision," *J. Geophys. Res.*, 86, pp. 1647–1651, 1981.

6. Thomas, J. B., *An Analysis of Long Baseline Radio Interferometry*, Technical Report 32–1526; Vol. VII, 37–50; Vol. VIII, 29–38; Vol. XVI, 47–64, Jet Propulsion Laboratory, Pasadena, Calif., 1972.

7. Thomas, J. B., *An Analysis of Radio Interferometry With the Block 0 System*, Publication 81–49, Jet Propulsion Laboratory, Pasadena, Calif., 1981.

8. Rogers, A. E. E., "Very-Long-Baseline Interferometry with Large Effective Bandwidth for Phase-Delay Measurements," *Radio Science*, 5, 1239–1247, 1970.

9. Fanselow, J. L., "Observation Model and Parameter Partials for the JPL VLBI Parameter Estimation Software MASTERFIT–V1.0," Jet Propulsion Laboratory, Pasadena, Calif., 1983 (to be published).

10. Kaplan, G. H., "The IAU Resolutions on Astronomical Constants, Time Scales, and the Fundamental Reference Frame," USNO Circular No. 163, United States Naval Observatory, Washington, D.C., 1981.

11. Lieske, J. H., et al., "Expressions for the Precession Quantities Based Upon the IAU (1976) System of Astronomical Constants," *Astron. Astrophys.* 58, pp. 1–16, 1977.

12. Wahr, J. M., "The Forced Nutations of an Elliptical, Rotating, Elastic and Oceanless Earth," *Geophys. J. Roy. Astron. Soc.*, 64, 705, 1981.

13. Seidelmann, P. K., "1980 IAU Theory of Nutation: The Final Report of the IAU Working Group on Nutation," *Celestial Mechanics*, 27, pp. 79–106, 1982.

14. Aoki, S., et al., "The New Definition of Universal Time," *Astron. Astrophys.* 105, pp. 359–361, 1982.

15. Standish, E. M., "Orientation of the JPL Ephemerides, DE200/LE200, to the Dynamical Equinox of J2000," *Astron. Astrophys.*, 114, pp. 297–302, 1982.

16. Chao, C. C., *The Tropospheric Calibration Model for Mariner Mars 1971*, Technical Report 32–1587, pp. 61–76, Jet Propulsion Laboratory, Pasadena, Calif., 1974.

17. Klobuchar, J. A., and Malik, C. A., *Geophysics and Space Data Bulletin*, Vol. 9, No. 2, pp. 311–318, A. L. Carrigan, ed.; AFCRL-72-0502, Special Report No. 145, Air Force Cambridge Research Laboratories, L. G. Hanscom Field, Mass., 1972.

18. Wallace, K. S., private communication, 1982.

19. Moyer, T. D., private communication, 1981.

20. Ma, C., Clark, T. A., and Shaffer, D. B., Mark III VLBI: Astrometry and Epoch J2000.0, Bull. AAS 13, 899, 1982.

21. Ma, C., private communication, 1982.

22. Rogers, A. E. E., et al., "Very-Long-Baseline Interferometry: The Mark III System for Geodesy, Astrometry and Aperture Synthesis," *Science*, 219, pp. 51–54, 1983.

23. Rius, A. and Calera, E., private communication, 1982.

24. Morabito, D. D., Claflin, E. S., and Steinberg, C. J., "VLBI Detection of Crustal Plate Motion Using DSN Antennas as Base Stations," *DSN Progress Report 42-56*, pp. 59-75 Jet Propulsion Laboratory, Pasadena, Calif., 1980.

25. Minster, J. B., and Jordan, T. H., "Present-Day Plate Motions," *J. Geophys. Res.*, 83, pp. 5331-5354, 1978.

26. Anderle, R. J., and Malyevac, C. A., "Current Plate Motions Based on Doppler Satellite Observations," *Geophys. Res. Lett.*, 10, p. 67, 1983.

27. Bureau International de l'Heure, *Annual Report for 1981*, Paris, France, 1981.

28. Fliegel, H. F., Dickey, J. O., and Williams, J. G., "Intercomparison of Lunar Laser and Traditional Determinations of Earth Rotation," pp. 53-88 *IAU Colloquium Proc.* No. 63, O. Calame, ed., Grasse, France, 1981.

29. Capitaine, N., and Feissel, M., "The Introduction of the IAU 1980 Nutation Theory in the Computation of the Earth Rotation Parameters by the Bureau International de l'Heure, a Proposal," *Bull. Geodesique*, 1982 (to be published).

30. Dickey, J. O., and Williams, J. G., "Geophysical Applications of Lunar Laser Ranging," *Eos*, 63, 301, 1982.

31. Wahr, J. M., "The Tidal Motions of a Rotating, Elastic and Oceanless Earth," pp. 162-171, Thesis, University of Colorado, 1977.

32. Lambeck, K., *The Earth's Variable Rotation: Geophysical Causes and Consequences*, pp. 13, 111, Cambridge, Cambridge U. Press, 1980.

33. Will, C. M., "The Confrontation Between General Relativity and Experiment," *Ann. N.Y. Acad. Sci.*, 336, pp. 307-321, 1980.

Table 1. Characteristics of antennas used in 1971–1980 VLBI observations

Antenna	Location	Diameter (m)	Efficiency		Zenith system temperature (K)	
			S	X	S	X
DSS11	Goldstone, Calif.	26	0.55	-	35	-
DSS13	Goldstone, Calif.	26	0.58	0.45	35	35
DSS14	Goldstone, Calif.	64	0.56	0.43	25	25
DSS43	Tidbinbilla, Australia	64	0.56	0.43	25	25
DSS62	Madrid, Spain	26	0.58	-	35	-
DSS63	Madrid, Spain	64	0.56	0.43	25	25
OVRO	Big Pine, Calif.	40	-	0.45	-	200
HAYST	Westford, Mass.	37	-	0.40	-	75

Table 2. Summary of 1971–1980 VLBI observing sessions

Date	Antennas	Session length (hr)	No. of distinct sources	No. of obs.	Observable type *	Freq. bands	Freq. standard **
71/ 8/28	14-62	15	17	43	DR	S	H,H
71/ 9/ 1	14-62	15	13	24	DR	S	H,H
71/ 9/ 6	14-62	17.5	15	45	DR	S	H,H
71/ 9/10	14-62	15	15	45	DR	S	H,H
73/ 4/30	14-62	8	12	21	DR	S	H,Rb
73/ 9/ 8	14-62	8	7	17	DR	S	H,Rb
74/ 2/15	14-62	6.5	8	20	DR	S	H,Rb
74/ 4/21	14-62	8	10	20	DR	S	H,Rb
74/ 6/21	14-62	6	10	17	DR	S	H,Rb
74/ 8/ 6	14-62	5	3	7	DR	S	H,Rb
77/ 1/12	11-43	2	9	12	D+DR	S	Rb,H
77/ 1/21	11-14-43	4.5	20	43	D+DR	S	Rb,H,H
77/ 1/31	14-63	6	15	26	D+DR	S	H,Rb
77/ 2/ 1	11-43	5.5	16	23	D+DR	S	Rb,H
77/ 2/13	11-14-43	10	24	68	D+DR	S	Rb,H,H
77/ 2/28	11-14-43	10	25	64	D+DR	S & X	Rb,H,H
77/ 4/13	14-63	7.5	19	44	D+DR	S	H,Rb
78/ 1/14	14-43	14	24	50	D+DR	X	H,H
78/ 1/24	14-43	6	19	36	D+DR	X	H,Rb
78/ 2/12	14-43	8	18	44	D+DR	X	H,H
78/ 2/24	OV-HY	48	8	123	D+DR	X	H,H
78/ 5/15	14-43	10	23	58	D+DR	X	Cs,H
78/ 7/30	14-63	9	25	47	D+DR	S	H,H
78/ 9/ 3	14-43	5	19	29	D+DR	S/X	H,Rb
78/ 9/ 4	14-63	9	13	25	D+DR	S	H,H
78/10/27	14-43	18.5	45	97	D+DR	S/X	H,H
78/10/30	14-63	8	22	32	D+DR	S/X	H,Cs
78/11/ 4	14-43	3.5	15	23	D+DR	S/X	H,H
78/11/ 5	14-63	23	30	60	D+DR	S/X	H,Cs
78/12/31	14-43	22.5	48	117	D+DR	S/X	H,H
79/ 6/ 6	13-14	3.5	13	15	D+DR	S	H,H
79/ 7/21	13-14	4.5	23	30	D+DR	S	H,H
79/ 8/26	13-14	6	24	31	D+DR	S	H,H
79/ 9/18	13-14	5	22	35	D+DR	S	H,H
79/11/15	62-63	4.5	16	25	D+DR	S	Rb,H
79/11/23	14-43	9	21	39	D+DR	S/X	H,H
79/11/25	14-63	20.5	46	113	D+DR	S/X	H,H
79/12/20	14-43	23	60	137	D+DR	S/X	H,H
79/12/21	14-63	10	16	33	D+DR	S/X	H,H
79/12/27	14-63	23	30	66	D+DR	S/X	H,H
79/12/29	14-43	8.5	21	45	D+DR	S/X	H,H
80/ 1/12	14-43	20	52	110	D+DR	S/X	H,H
80/ 1/25	14-63	20.5	26	47	D+DR	S/X	H,H
80/ 1/27	14-43	8.5	22	42	D+DR	S/X	H,H
80/ 2/13	14-63	23	52	137	D+DR	S/X	H,H
80/ 2/14	14-43	8.5	25	50	D+DR	S/X	H,H
80/ 2/23	14-43	20.5	54	99	D+DR	S/X	H,H
80/ 2/24	14-63	8.5	24	48	D+DR	S/X	H,H
Total			117	2382			

* D = delay, DR = delay rate.
** Rb = rubidium, Cs = cesium, H = hydrogen maser.

Table 3. JPL 1983–2 radio source catalog (J2000.0)

	IAU designation	Common name	Average obs. epoch	No. of sessions	Observations Delay	Delay rate	Right ascension h	m	s	Error(σ)	Declination d	m	s	Error(σ)
	0008-264	P 0008-264	1980.05	3	8	8	0	11	1.24747	0.00039	-26	12	33.3891	0.0053
	0104-408	P 0104-408	1979.43	7	21	21	1	6	45.10824	0.00023	-40	34	19.9640	0.0035
	0106+013	P 0106+01	1978.39	23	38	46	1	8	38.77105	0.00011	1	35	0.3174	0.0026
	0111+021	P 0111+021	1980.04	3	6	6	1	13	43.14505	0.00168	2	22	17.3155	0.0254
	0113-118	P 0113-118	1978.85	5	12	12	1	16	12.52214	0.00067	-11	36	15.4375	0.0103
	0133+476	DA 55	1979.14	20	41	43	1	36	58.59495	0.00018	47	51	29.1053	0.0013
S	0134+329	3C 48	1979.64	3	3	3	1	37	41.34210	0.05828	33	9	35.4968	0.3769
	0202+149	P 0202+14	1980.02	6	13	13	2	4	50.41405	0.00012	15	14	11.0461	0.0024
	0224+671	DW 0224+67	1977.48	24	39	62	2	28	50.05199	0.00032	67	21	3.0339	0.0019
	0234+285	CTD 20	1980.02	6	13	13	2	37	52.40585	0.00014	28	48	8.9942	0.0021
	0235+164	GC 0235+16	1980.04	6	11	11	2	38	38.93026	0.00012	16	36	59.2767	0.0023
R	0237-233	P 0237-23	1980.02	2	3	3	2	40	8.17472	0.00091	-23	9	15.7416	0.0126
	0300+470	OE 400	1978.39	10	19	19	3	3	35.24246	0.00024	47	16	16.2831	0.0019
	0316+413	3C 84	1978.72	10	11	16	3	19	48.16043	0.00019	41	30	42.1074	0.0019
	0332-403	P 0332-403	1977.84	5	17	17	3	34	13.65384	0.00037	-40	8	25.3969	0.0044
	0333+321	NRAO 140	1977.61	25	34	50	3	36	30.10794	0.00016	32	18	29.3448	0.0017
	0336-019	CTA 26	1979.52	9	13	15	3	39	30.93773	0.00013	-1	46	35.8004	0.0029
	0355+508	NRAO 150	1978.60	6	26	26	3	59	29.74801	0.00026	50	57	50.1688	0.0022
	0402-362	P 0402-362	1978.07	4	11	11	4	3	53.74941	0.00044	-36	5	1.9132	0.0054
	0406+121	GC 0406+12	1980.03	6	12	12	4	9	22.00860	0.00014	12	17	39.8426	0.0055
	0420-014	P 0420-01	1977.97	11	19	20	4	23	15.80052	0.00020	-1	20	33.0642	0.0037
	0420+417	VRO 41.04.01	1979.72	7	9	10	4	23	56.01004	0.00026	41	50	2.7185	0.0033
S	0429+415	3C 119	1979.66	3	3	2	4	32	36.48682	0.28126	41	38	28.7574	1.6483
	0430+052	3C 120	1977.28	15	16	24	4	33	11.09592	0.00025	5	21	15.6142	0.0040
	0434-188	P 0434-188	1980.02	3	5	5	4	37	1.48289	0.00057	-18	44	48.6198	0.0086
	0438-436	P 0438-43	1977.87	5	20	20	4	40	17.17941	0.00033	-43	33	8.6054	0.0040
	0440-003	NRAO 190	1976.36	19	16	34	4	42	38.66089	0.00051	-0	17	43.4243	0.0080
	0451-282	P 0451-28	1980.02	3	5	5	4	53	14.64585	0.00048	-28	7	37.3195	0.0062
S	0518+165	3C 138	1979.55	1	2	2	5	21	10.04094	0.11462	16	38	21.9327	0.5140
	0528+134	P 0528+134	1980.03	7	14	14	5	30	56.41692	0.00012	13	31	55.1501	0.0022
	0537-441	P 0537-441	1978.46	9	20	20	5	38	50.36073	0.00028	-44	5	8.9386	0.0037
	0552+398	DA 193	1977.55	17	27	33	5	55	30.80616	0.00022	39	48	49.1667	0.0019
	0605-085	P 0605-08	1978.96	4	6	6	6	7	59.69940	0.00070	-8	34	49.9881	0.0100
	0607-157	P 0607-15	1978.52	12	18	18	6	9	40.94952	0.00025	-15	42	40.6778	0.0044
	0723-008	DW 0723-00	1979.99	5	8	8	7	25	50.63977	0.00020	-0	54	56.5434	0.0038
	0727-115	P 0727-11	1977.93	12	20	21	7	30	19.11287	0.00024	-11	41	12.6140	0.0043
	0735+178	P 0735+17	1977.85	16	20	24	7	38	7.39401	0.00022	17	42	18.9934	0.0036
	0738+313	OI 363	1977.01	14	14	23	7	41	10.70377	0.00043	31	12	0.2264	0.0054
	0742+103	DW 0742+10	1978.21	22	45	49	7	45	33.05953	0.00013	10	11	12.6897	0.0023
	0748+126	P 0748+126	1980.00	5	10	10	7	50	52.04562	0.00017	12	31	4.8263	0.0031
	0814+425	OJ 425	1977.83	19	23	27	8	18	16.00000	0.00023	42	22	45.4144	0.0018
	0823+033	P 0823+033	1980.01	8	13	13	8	25	50.33852	0.00018	3	9	24.5130	0.0033
	0827+243	B2 0827+24	1979.76	8	10	11	8	30	52.08663	0.00034	24	10	59.8105	0.0044
R	0831+557	4C 55.16	1977.58	6	4	7	8	34	54.90177	0.00182	55	34	21.1328	0.0228
	0836+710	4C 71.07	1979.64	8	15	15	8	41	24.36807	0.00043	70	53	42.1772	0.0020
	0851+202	OJ 287	1978.04	15	37	41	8	54	48.87506	0.00013	20	6	30.6363	0.0018
	0859-140	P 0859-14	1977.80	11	16	16	9	2	16.83076	0.00081	-14	15	30.8847	0.0123
	0859+470	OJ 499	1977.92	5	6	6	9	3	3.99136	0.00076	46	51	4.1266	0.0051
	0923+392	4C 39.25	1978.52	29	78	83	9	27	3.01394	0.00013	39	2	20.8497	0.0012
	0952+179	AO 0952+17	1979.98	5	5	5	9	54	56.82357	0.00078	17	43	31.2228	0.0126
	1004+141	GC 1004+14	1980.01	6	16	15	10	7	41.49848	0.00047	13	56	29.5911	0.0063
	1034-293	P 1034-293	1980.00	6	10	10	10	37	16.07921	0.00030	-29	34	2.8183	0.0042
	1038+064	OL 064.5	1980.01	2	6	6	10	41	17.16237	0.00020	6	10	16.9218	0.0382
	1040+123	3C 245	1980.03	6	7	6	10	42	44.60596	0.00036	12	3	31.2536	0.0049
	1055+018	P 1055+01	1979.73	10	23	25	10	58	29.60516	0.00011	1	33	58.8174	0.0025
	1104-445	P 1104-445	1977.74	10	15	15	11	7	8.69332	0.00047	-44	49	7.6227	0.0047
	1111+149	GC 1111+14	1980.03	6	11	11	11	13	58.69532	0.00048	14	42	26.9449	0.0061
R	1116+128	P 1116+12	1980.11	3	4	4	11	18	57.30154	0.00031	12	34	41.7093	0.0064

Table 3 (contd)

	IAU designation	Common name	Average obs. epoch	No. of sessions	Observations Delay	Observations Delay rate	Right ascension h	m	s	Error(σ)	Declination d	m	s	Error(σ)
	1123+264	P 1123+26	1980.02	8	21	21	11	25	53.71196	0.00019	26	10	19.9738	0.0023
	1127-145	P 1127-14	1978.70	22	51	51	11	30	7.05233	0.00016	-14	49	27.3941	0.0033
R	1128+385	GC 1128+38	1980.15	1	3	3	11	30	53.28215	0.00047	38	15	18.5471	0.0037
R	1130+009	P 1130+009	1980.05	3	3	3	11	33	20.05385	0.00741	0	40	53.4607	2.2108
	1144-379	P 1144-379	1978.73	15	40	40	11	47	1.37021	0.00022	-38	12	11.0305	0.0034
	1148-001	P 1148-00	1978.09	10	15	15	11	50	43.87056	0.00040	-0	23	54.2102	0.0064
	1222+037	P 1222+037	1980.03	7	13	13	12	24	52.42221	0.00021	3	30	50.2808	0.0038
	1226+023	3C 273	1978.62	20	54	57	12	29	6.69970	0.00000	2	3	8.5914	0.0025
	1228+126	3C 274	1980.04	7	12	12	12	30	49.42342	0.00031	12	23	28.0376	0.0043
	1244-255	P 1244-255	1980.02	6	16	16	12	46	46.80184	0.00025	-25	47	49.2757	0.0037
	1253-055	3C 279	1978.24	6	14	14	12	56	11.16647	0.00038	-5	47	21.5321	0.0063
	1308+326	B2 1308+32	1980.02	10	24	24	13	10	28.66381	0.00013	32	20	43.7788	0.0015
	1313-333	OP-322	1978.15	9	16	16	13	16	7.98528	0.00031	-33	38	59.1782	0.0041
	1334-127	DW 1335-12	1977.96	10	20	21	13	37	39.78288	0.00028	-12	57	24.7031	0.0043
	1342+663	GC 1342+663	1980.12	3	5	5	13	44	8.67956	0.00053	66	6	11.6365	0.0025
R	1349-439	P 1349-439	1980.11	2	4	4	13	52	56.53523	0.00061	-44	12	40.4008	0.0057
	1354+195	P 1354+19	1980.02	11	22	22	13	57	4.43660	0.00017	19	19	7.3665	0.0027
	1418+546	GC 1418+54	1980.13	2	6	6	14	19	46.59754	0.00019	54	23	14.7823	0.0015
	1430-178	OQ-151	1980.05	4	9	9	14	32	57.68946	0.00054	-18	1	35.2438	0.0080
S	1458+718	3C 309 1	1979.61	4	7	7	14	59	7.33716	0.12838	71	40	20.4458	0.6309
	1502+106	OR 103	1979.35	18	39	40	15	4	24.97966	0.00011	10	29	39.1945	0.0023
	1510-089	P 1510-08	1978.18	6	15	15	15	12	50.53332	0.00051	-9	5	59.8409	0.0079
	1519-273	P 1519-273	1980.03	6	15	15	15	22	37.67552	0.00022	-27	30	10.7889	0.0035
	1555+001	DW 1555+00	1976.86	14	22	34	15	57	51.43418	0.00033	-0	1	50.4203	0.0052
	1611+343	DA 406	1977.37	16	30	44	16	13	41.06409	0.00025	34	12	47.9082	0.0026
	1633+382	GC 1633+38	1980.04	10	32	32	16	35	15.49283	0.00013	38	8	4.4985	0.0013
	1638+398	NRAO 512	1979.50	16	54	53	16	40	29.63258	0.00015	39	46	46.0278	0.0014
	1641+399	3C 345	1978.28	19	54	72	16	42	58.80983	0.00013	39	48	36.9928	0.0012
	1656+053	DW 1656+05	1978.85	9	12	16	16	58	33.44733	0.00061	5	15	16.4383	0.0093
	1717+178	GC 1717+17	1980.07	8	19	19	17	19	13.04837	0.00022	17	45	6.4352	0.0037
	1730-130	NRAO 530	1979.13	14	28	28	17	33	2.70553	0.00018	-13	4	49.5460	0.0038
	1738+476	OT 465	1978.70	4	6	6	17	39	57.12566	0.00078	47	37	58.3768	0.0045
	1741-038	P 1741-038	1977.44	13	25	35	17	43	58.85676	0.00027	-3	50	4.6252	0.0046
	1749+701	1749+701	1979.45	11	16	16	17	48	32.83875	0.00060	70	5	50.7750	0.0032
	1807+698	3C 371	1978.96	18	48	57	18	6	50.67971	0.00026	69	49	28.1088	0.0010
	1821+107	P 1821+10	1980.06	7	14	14	18	24	2.85524	0.00013	10	44	23.7698	0.0048
S	1901+319	3C 395	1979.61	4	5	5	19	2	55.83921	0.08749	31	59	40.3952	0.7978
	1921-293	OV-236	1978.47	4	11	9	19	24	51.05564	0.00044	-29	14	30.1133	0.0055
	1933-400	P 1933-400	1979.86	4	7	7	19	37	16.21675	0.00059	-39	58	1.5528	0.0061
	1958-179	OV-198	1979.30	8	18	17	20	0	57.09073	0.00037	-17	48	57.6761	0.0055
	2021+614	OW 637	1978.47	11	18	19	20	22	6.68158	0.00095	61	36	58.8193	0.0055
	2029+547	OW 551	1980.02	3	8	8	20	31	47.95842	0.00040	54	55	3.1495	0.0037
	2030+121	P 2029+121	1980.06	9	14	14	20	31	54.99410	0.00019	12	19	41.3436	0.0034
S	2037+511	3C 418	1979.64	3	5	5	20	38	36.94366	0.06543	51	19	11.8561	0.4130
	2113+293	B2 2113+29B	1979.83	11	19	19	21	15	29.41343	0.00015	29	33	38.3663	0.0024
	2134+004	P 2134+004	1977.17	14	26	40	21	36	38.58616	0.00017	0	41	54.2150	0.0038
	2145+067	P 2145+06	1978.52	21	31	39	21	48	5.45853	0.00011	6	57	38.6057	0.0023
	2149+056	OX 082	1980.06	8	16	16	21	51	37.87530	0.00017	5	52	12.9556	0.0034
	2155-152	OX-192	1978.66	4	6	6	21	58	6.28154	0.00072	-15	1	9.3263	0.0109
	2200+420	VRO 42.22.01	1978.05	27	46	60	22	2	43.29125	0.00016	42	16	39.9839	0.0014
	2230+114	CTA 102	1978.45	10	13	13	22	32	36.40897	0.00050	11	43	50.9052	0.0068
	2234+282	GC 2234+28	1980.04	10	23	22	22	36	22.47076	0.00013	28	28	57.4168	0.0018
	2243-123	OY-172.6	1979.27	14	22	22	22	46	18.23184	0.00014	-12	6	51.2764	0.0033
	2245-328	P 2245-328	1979.55	7	20	20	22	48	38.68551	0.00024	-32	35	52.1861	0.0036
	2251+158	3C 454.3	1977.56	17	37	50	22	53	57.74779	0.00015	16	8	53.5658	0.0027
	2253+417	GC 2253+41	1980.11	3	11	11	22	55	36.70799	0.00019	42	2	52.5370	0.0030
	2320-035	P 2320-035	1980.00	5	8	7	23	23	31.95363	0.00021	-3	17	5.0216	0.0044
	2345-167	P 2345-16	1977.98	16	20	24	23	48	2.60846	0.00035	-16	31	12.0233	0.0052
S	2352+495	DA 611	1979.66	3	5	5	23	55	9.45244	0.07304	49	50	8.4831	0.2230

* In barycentric coordinates.
S Short-baseline data only.
R Inadequate redundancy fewer than 5 delay observations.

Table 4. Root-mean-square residuals for 1971–1980 observing sessions in the standard fit

Date	Antennas	RMS residuals Delay (ns)	RMS residuals Delay rate (psec/sec)
71/ 8/28	14-62	-	0.27
71/ 9/ 1	14-62	-	0.16
71/ 9/ 6	14-62	-	0.26
71/ 9/10	14-62	-	0.33
73/ 4/30	14-62	-	0.26
73/ 9/ 8	14-62	-	0.45
74/ 2/15	14-62	-	0.26
74/ 4/21	14-62	-	0.33
74/ 6/21	14-62	-	0.43
74/ 8/ 6	14-62	-	0.28
77/ 1/12	11-43	0.52	0.74
77/ 1/21	11-14-43	0.62	0.36
77/ 1/31	14-63	0.87	0.34
77/ 2/ 1	11-43	0.75	0.56
77/ 2/13	11-14-43	0.84	0.33
77/ 2/28	11-14-43	0.77	0.32
77/ 4/13	14-63	0.97	0.34
78/ 1/14	14-43	0.29	0.17
78/ 1/24	14-43	0.35	0.37
78/ 2/12	14-43	0.18	0.63
78/ 2/24	OV-HY	0.29	0.05
78/ 5/15	14-43	0.48	0.66
78/ 7/30	14-63	0.64	0.45
78/ 9/ 3	14-43	0.44	0.50
78/ 9/ 4	14-63	1.03	0.41
78/10/27	14-43	0.46	0.14
78/10/30	14-63	0.49	0.83
78/11/ 4	14-43	0.25	0.10
78/11/ 5	14-63	0.73	0.85
78/12/31	14-43	0.34	0.14
79/ 6/ 6	13-14	0.22	0.16
79/ 7/21	13-14	0.17	0.11
79/ 8/26	13-14	0.10	0.09
79/ 9/18	13-14	0.14	0.06
79/11/15	62-63	0.09	0.19
79/11/23	14-43	0.53	0.20
79/11/25	14-63	0.57	0.13
79/12/20	14-43	0.50	0.14
79/12/21	14-63	0.56	0.11
79/12/27	14-63	0.46	0.13
79/12/29	14-43	0.49	0.11
80/ 1/12	14-43	0.44	0.21
80/ 1/25	14-63	0.48	0.08
80/ 1/27	14-43	0.43	0.15
80/ 2/13	14-63	0.50	0.10
80/ 2/14	14-43	0.32	0.12
80/ 2/23	14-43	0.42	0.14
80/ 2/24	14-63	0.40	0.11
Average		0.52	0.30

Table 5. Source position repeatability results

Source	Average epoch		* Difference (mas)		RSS errors (mas)		Diff/RSS	
	Part 1	Part 2	RA	Dec	RA	Dec	RA	Dec
P 0104-408	78.74	80.06	-1.6	2.2	4.8	5.5	-0.33	0.40
P 0106+01	77.24	79.93	1.8	-0.4	4.7	5.4	0.38	-0.07
DA 55	77.74	79.92	3.2	3.7	3.9	3.0	0.83	1.23
DW 0224+67	76.34	79.84	0.6	-1.2	3.6	4.1	0.18	-0.29
NRAO 140	75.86	79.94	-1.8	3.9	4.4	3.7	-0.40	1.05
DW 0742+10	77.73	80.00	5.6	-6.7	4.0	4.3	1.40	-1.55
4C 39.25	77.85	80.02	2.2	0.3	2.6	2.3	0.84	0.13
P 1127-14	77.98	80.01	1.7	0.4	4.6	5.7	0.37	0.07
P 1144-379	78.12	80.00	0.0	-0.2	4.5	5.2	0.00	-0.04
OR 103	77.95	80.00	1.8	1.4	7.3	7.6	0.24	0.18
NRAO 512	77.83	80.04	-4.2	2.7	5.2	5.0	-0.80	0.54
3C 345	76.06	80.01	-1.5	0.8	3.3	3.5	-0.46	0.23
NRAO 530	78.31	79.95	-1.9	12.1	7.1	7.9	-0.27	1.54
3C 371	77.09	79.98	-6.6	2.2	4.9	4.1	-1.34	0.54
P 2145+06	76.62	80.03	-0.9	2.4	4.8	5.3	-0.19	0.45
VRO 42.22.01	76.82	79.92	-0.6	3.9	3.4	3.0	-0.16	1.31
OY-172.6	78.64	80.02	3.5	-4.0	5.0	6.0	0.71	-0.66
		RMS =	2.9	4.0		χ^2/N =	0.43	0.63

* Difference : 1971-78 position minus 1979-80 position.

Table 6. Station locations from 1971–1980 VLBI data

Station	CIO cylindrical coordinates		
	Equatorial (m)	Longitude (degrees)	Polar (m)
DSS11	5206339.890±0.562	243.1505770±0.0000055	3673763.464±0.322
DSS13	5215483.938 0.022	243.2051172 0.0000001	3660956.516 0.019
* DSS14	5203996.766 -	243.1104671 -	3677052. -
DSS43	5205251.060 0.087	148.9812611 0.0000010	-3674749.217 0.141
DSS62	4860817.898 0.162	355.6321691 0.0000028	4116905.731 0.250
DSS63	4862451.030 0.158	355.7519856 0.0000028	4115108.644 0.249
OVRO	5085449.442 0.093	241.7172850 0.0000010	3838603.826 0.092
HAYST	4700479.623 0.109	288.5118354 0.0000012	4296882.190 0.115

* Reference station.

Table 7. Selected baselines from 1971–1980 VLBI data

Baseline	CIO rectangular coordinates (m)			Length (m)
	x	y	z	
DSS14-DSS43	-2107273.066±0.117	7323703.098±0.042	-7351801.217±0.141	10588966.331±0.101
DSS14-DSS63	7202713.569 0.141	4281160.656 0.248	438056.644 0.249	8390429.843 0.043
OVRO-HAYST	3902005.520 0.027	21082.369 0.064	458278.364 0.069	3928881.596 0.025
DSS14-DSS11	2191.480 0.628	-3737.042 0.412	-3288.537 0.322	5438.983 0.301
DSS14-DSS13	2492.103 0.014	-14135.491 0.020	-16095.484 0.019	21565.883 0.013
DSS62-DSS63	2392.199 0.034	10015.216 0.013	-1797.088 0.023	10452.593 0.016

Table 8. Baseline formal uncertainties* from fit to 1971–1980 VLBI data

Baseline	Formal uncertainty (cm) x	y	z	Length
DSS11-DSS13	62.8	41.2	32.3	32.2
DSS14	62.8	41.2	32.2	30.1
DSS43	63.9	41.2	34.9	38.0
DSS62	64.4	48.2	40.8	66.8
DSS63	64.3	48.1	40.7	66.7
OVRO	63.5	42.2	33.5	30.7
HAYST	63.5	42.7	34.2	63.9
DSS13-DSS14	1.4	2.0	1.9	1.3
DSS43	11.8	4.7	14.2	10.3
DSS62	14.5	24.9	25.1	5.6
DSS63	14.1	24.9	25.0	4.7
OVRO	(9.0	9.0	9.0	9.0)
HAYST	9.4	11.1	11.3	9.3
DSS14-DSS43	11.7	4.2	14.1	10.1
DSS62	14.5	24.8	25.0	5.3
DSS63	14.1	24.8	24.9	4.3
OVRO	9.1	9.2	9.2	9.1
HAYST	9.5	11.2	11.5	9.4
DSS43-DSS62	16.4	25.6	31.4	32.1
DSS63	16.1	25.6	31.3	31.9
OVRO	14.9	10.1	16.8	13.8
HAYST	14.9	12.5	19.8	15.4
DSS62-DSS63	3.4	1.3	2.3	1.6
OVRO	17.1	26.5	26.7	10.6
HAYST	17.2	26.0	26.0	15.5
DSS63-OVRO	16.8	26.4	26.6	10.2
HAYST	16.9	26.0	25.9	15.4
OVRO-HAYST	2.7	6.4	6.9	2.5

* In CIO rectangular coordinates.

Table 9. Polar motion and UT1 values* from 1971–1980 VLBI data

Date	Mean Julian date	Polar motion, mas x		Polar motion, mas y		UT1-UTC, msec	
1971/ 8/29	41192.17					-76.7	± 1.3
1971/ 9/ 2	41196.19					-76.0	1.4
1971/ 9/ 7	41201.14					-82.1	1.2
1971/ 9/11	41205.08					-82.6	1.6
1973/ 4/30	41802.87					405.0	2.0
1973/ 9/ 8	41933.85					54.2	3.1
1974/ 2/16	42094.06					577.6	1.9
1974/ 4/21	42158.83					383.4	2.4
1974/ 6/21	42219.58					215.7	3.6
1974/ 8/ 6	42265.87					113.2	4.1
1977/ 1/12	43155.59			100.7	± 8.8	632.3	2.4
1977/ 1/21	43164.43			122.8	6.5	605.6	1.4
1977/ 1/31	43174.34					577.9	0.9
1977/ 1/31	43174.84	-171.0	±15.2	151.3	8.3		
1977/ 2/ 1	43175.44					577.8	2.4
1977/ 2/13	43187.31			190.4	5.9	544.4	1.2
1977/ 2/28	43202.19			240.6	3.1	500.3	0.8
1977/ 4/13	43246.23	-184.6	14.1			362.3	0.8
1978/ 1/14	43522.67			21.5	3.0	602.0	0.8
1978/ 1/24	43532.16			38.0	3.1	576.2	0.8
1978/ 2/12	43551.56			72.7	3.0	511.1	0.7
1978/ 2/25	43564.92	-177.2	...	114.6	...	467.2	...
1978/ 5/15	43643.53			389.0	3.2	203.1	0.8
1978/ 7/31	43720.16	72.2	15.8			25.5	0.9
1978/ 9/ 3	43754.89					-53.5	1.8
1978/ 9/ 4	43755.42	166.9	25.4	422.0	7.4		
1978/ 9/ 4	43755.70					-53.8	1.1
1978/10/28	43809.02					-205.5	0.7
1978/10/28	43809.58	240.8	9.1	256.9	2.7		
1978/10/30	43811.20					-212.0	0.7
1978/11/ 4	43816.76					-229.1	0.6
1978/11/ 5	43817.84	241.5	7.6	223.2	2.3		
1978/11/ 6	43818.18					-233.8	0.5
1978/12/31	43873.44			86.8	2.9	-400.7	0.7
1979/11/23	44200.80					-256.6	0.6
1979/11/25	44202.64	130.9	5.9	320.5	2.3		
1979/11/26	44203.30					-261.7	0.5
1979/12/20	44227.56					-325.7	...
1979/12/20	44227.78	139.4	...	273.1	...		
1979/12/21	44228.71					-328.2	...
1979/12/27	44234.79					-343.8	0.5
1979/12/28	44235.54	134.3	6.5	259.7	2.0		
1979/12/29	44236.66					-349.3	0.5
1980/ 1/12	44250.83			237.3	2.9	616.0	0.7
1980/ 1/26	44264.00					581.0	0.5
1980/ 1/26	44264.75	110.2	7.1	214.1	2.2		
1980/ 1/27	44265.62					576.6	0.6
1980/ 2/14	44283.21					539.8	0.5
1980/ 2/14	44283.40	73.1	5.7	191.2	1.7		
1980/ 2/14	44283.92					537.4	0.4
1980/ 2/23	44292.85					510.9	0.5
1980/ 2/24	44293.04	58.3	6.4	184.5	1.9		
1980/ 2/24	44293.54					510.3	0.5

* These UT values include short-period tidal effects.

Table 10. Zenith tropospheric delays from 1971–1980 VLBI data

Station	Date	Mean Julian date	Zenith delay (cm)
DSS11	77/ 1/12	43155.59	207.3 ± 5.3
	77/ 1/21	43164.48	212.6 4.3
	77/ 2/ 1	43175.44	210.3 4.9
	77/ 2/13	43187.33	216.1 4.1
	77/ 2/28	43202.11	211.1 5.9
DSS14	71/ 8/29	41192.17	222.0 ± 4.0
	71/ 9/ 2	41196.19	214.0 3.9
	71/ 9/ 7	41201.14	214.2 4.0
	71/ 9/11	41205.08	213.3 4.2
	73/ 4/30	41802.87	209.8 5.5
	73/ 9/ 8	41933.85	211.7 5.5
	74/ 2/16	42094.06	211.2 5.5
	74/ 4/21	42158.83	206.8 4.8
	74/ 6/21	42219.58	211.8 5.9
	74/ 8/ 6	42265.87	216.3 5.9
	77/ 1/21	43164.39	213.1 5.0
	77/ 1/31	43174.34	200.6 2.8
	77/ 2/13	43187.30	215.9 4.1
	77/ 2/28	43202.20	208.9 1.6
	77/ 4/13	43246.23	209.0 1.8
	78/ 1/14	43522.67	215.8 1.2
	78/ 1/24	43532.16	209.5 1.7
	78/ 2/12	43551.56	208.5 0.6
	78/ 5/15	43643.53	210.9 1.7
	78/ 7/31	43720.16	206.2 2.0
	78/ 9/ 3	43754.89	215.2 2.1
	78/ 9/ 4	43755.70	211.9 4.7
	78/10/28	43809.02	209.0 0.7
	78/10/30	43811.20	208.2 2.3
	78/11/ 4	43816.76	211.4 0.8
	78/11/ 5	43817.90	210.7 2.5
	78/11/ 6	43818.38	210.7 3.6
	78/12/31	43873.23	208.5 0.9
		43873.67	206.7 0.8
	79/11/23	44200.70	210.9 3.1
		44200.87	210.0 1.8
	79/11/26	44203.13	209.1 1.1
		44203.62	209.0 1.8
	79/12/20	44227.23	212.0 1.3
		44227.71	207.7 0.8
	79/12/21	44228.71	210.9 2.7
	79/12/27	44234.79	207.4 2.9
	79/12/29	44236.66	210.7 1.0
	80/ 1/12	44250.69	219.7 1.0
	80/ 1/13	44251.12	217.4 1.4
	80/ 1/25	44263.73	212.1 3.3
	80/ 1/26	44264.09	206.6 2.1
	80/ 1/27	44265.54	205.6 1.8
		44265.69	204.1 1.0
	80/ 2/13	44282.80	211.5 1.5
	80/ 2/14	44283.09	210.7 0.9
		44283.50	211.6 1.2
		44283.92	215.9 1.3
	80/ 2/23	44292.85	210.1 0.8
	80/ 2/24	44293.54	208.9 1.7

Table 10 (contd)

Station	Date	Mean Julian date	Zenith delay (cm)
DSS43	77/ 1/12	43155.59	226.5 ± 4.9
	77/ 1/21	43164.43	219.0 2.9
	77/ 2/ 1	43175.44	227.8 4.1
	77/ 2/13	43187.31	226.7 2.7
	77/ 2/28	43202.19	226.2 1.5
	78/ 1/14	43522.67	223.2 1.3
	78/ 1/24	43532.16	229.1 2.3
	78/ 2/12	43551.56	222.4 0.6
	78/ 5/15	43643.53	224.0 2.4
	78/ 9/ 3	43754.89	227.6 2.0
	78/10/28	43809.02	227.2 0.8
	78/11/ 4	43816.76	220.4 0.8
	78/12/31	43873.23	225.6 0.8
		43873.67	224.6 0.7
	79/11/23	44200.80	234.0 1.9
	79/12/20	44227.23	221.6 0.9
		44227.56	221.0 0.8
		44227.88	221.9 1.2
	79/12/29	44236.56	230.7 1.0
		44236.76	228.6 2.0
	80/ 1/12	44250.83	221.0 0.8
	80/ 1/27	44265.62	223.5 1.1
	80/ 2/14	44283.92	218.7 0.9
	80/ 2/23	44292.85	223.9 0.8
DSS62	71/ 8/29	41192.17	220.0 ± 4.4
	71/ 9/ 2	41196.19	227.0 4.3
	71/ 9/ 7	41201.14	225.2 4.6
	71/ 9/11	41205.08	231.0 4.9
	73/ 4/30	41802.87	223.0 5.5
	73/ 9/ 8	41933.85	224.7 5.5
	74/ 2/16	42094.06	218.6 4.7
	74/ 4/21	42158.83	223.4 5.5
	74/ 6/21	42219.58	224.3 5.5
	74/ 8/ 6	42265.87	230.1 5.7
DSS63	77/ 1/31	43174.34	215.7 ± 4.2
	77/ 4/13	43246.23	215.7 2.4
	78/ 7/31	43720.16	219.0 3.0
	78/ 9/ 4	43755.70	230.4 4.9
	78/10/30	43811.20	217.3 3.0
	78/11/ 5	43817.90	220.1 3.0
	78/11/ 6	43818.38	221.1 2.7
	79/11/26	44203.30	217.0 1.1
	79/12/21	44228.64	211.0 1.7
		44228.82	215.2 2.4
	79/12/27	44234.79	219.7 1.4
	80/ 1/26	44264.00	221.2 1.7
	80/ 2/13	44282.80	216.9 1.6
	80/ 2/14	44283.09	218.2 1.1
		44283.50	219.8 1.3
	80/ 2/24	44293.54	222.6 1.4
OVRO	78/ 2/25	43564.17	203.6 ± 1.7
		43564.67	205.0 1.2
	78/ 2/26	43565.03	196.6 3.1
		43565.50	202.0 1.7
HAYST	78/ 2/25	43564.17	228.4 ± 1.1
		43564.67	227.3 0.7
	78/ 2/26	43565.03	228.9 1.4
		43565.50	228.7 0.9

Table 11. Differential clock parameters* from 1971–1980 VLBI data

Station	Date	Epoch(ns)	Rate(psec/sec)	dR/dt(1/sec) *10**18
DSS11	77/ 2/13 7:49	-8604± 43	0.462±1.30	...
	77/ 2/28 2:38	-12740 19	-1.398 0.565	...
DSS13	79/ 6/ 6 7:15	-249±0.3	-1.091±0.020	...
	79/ 7/21 13:01	-219 0.1	-2.364 0.016	2.3 ± 1.6
	79/ 8/26 5:30	758 0.3	-1.126 0.013	...
	8:03	758 0.7	-1.075 0.048	...
	8:51	756 1.1	-1.283 0.098	...
	79/ 9/18 5:27	1620 0.2	-2.134 0.006	...
DSS14	77/ 1/21 9:15	1371± 3	0.249±0.280	...
	77/ 2/13 6:43	13 47	-0.613 1.65	...
	9:33	-41 43	-0.633 1.32	...
DSS43	77/ 1/12 14:06	-1479± 4	-3.295±0.240	...
	77/ 1/21 9:30	12170 2	-4.406 0.252	...
	12:49	12223 3	-4.596 0.257	...
	77/ 2/ 1 9:18	28444 4	-2.160 0.198	...
	12:02	28555 3	-1.978 0.328	...
	77/ 2/13 2:43	29245 22	-2.200 0.656	...
	6:46	29272 46	-3.207 1.49	...
	9:46	29275 43	-2.888 1.31	...
	77/ 2/28 3:18	29961 1	-2.334 0.019	...
	9:00	30047 1	-2.217 0.057	...
	78/ 1/14 8:47	24356 1	1.333 0.048	...
	16:03	24324 0.8	1.319 0.020	...
	19:31	24326 1	1.219 0.019	...
	78/ 1/24 3:49	19393 1	7.014 0.014	...
	78/ 2/12 13:21	15482 0.6	-1.054 0.008	-5.6 ± 0.5
	78/ 5/15 9:16	10130 1	0.989 0.039	...
	12:16	10128 1	0.760 0.029	...
	16:22	10125 1	1.243 0.028	...
	78/ 9/ 3 21:20	4539 1	-3.297 0.018	...
	78/10/27 19:26	8786 0.6	...	...
	78/10/28 0:23	...	2.018 0.006	...
	5:20	8786 0.6	...	...
	78/11/ 4 18:11	10306 0.7	2.028 0.012	...
	78/12/31 8:28	16003 0.6	0.211 0.004	...
	22:29	16010 1	0.126 0.028	...
	79/11/23 16:43	38096 2	-0.467 0.048	...
	19:50	38100 2	-0.285 0.147	...
	22:16	38138 1	-0.318 0.057	...
	79/12/20 13:22	36494 0.6	-0.577 0.003	...
	79/12/29 13:31	35896 0.7	-1.057 0.017	...
	18:08	35896 0.8	-1.061 0.019	...
	80/ 1/12 13:18	35904 0.7	0.305 0.009	...
	23:13	35905 0.6	0.357 0.006	...
	80/ 1/27 14:54	36511 0.8	0.810 0.014	...
	80/ 2/14 20:03	33524 0.9	-0.151 0.018	...
	80/ 2/15 0:33	33525 0.8	-0.131 0.015	...
	80/ 2/23 20:21	33349 0.6	-0.199 0.002	...

Table 11 (contd)

Station	Date	Epoch(ns)	Rate(psec/sec)	dR/dt(1/sec) *10**18
DSS62	71/ 8/29 4:11	...	-1.625±0.056	...
	71/ 9/ 2 4:29	...	-1.741 0.049	...
	71/ 9/ 7 3:16	...	-2.086 0.052	...
	71/ 9/10 22:46	...	-1.959 0.080	...
	71/ 9/11 5:44	...	-1.529 0.086	...
	73/ 4/30 17:52	...	-6.532 0.138	...
	22:03	...	-6.471 0.085	...
	73/ 9/ 8 20:25	...	6.622 0.138	...
	74/ 2/16 1:27	...	7.711 0.082	...
	74/ 4/21 19:52	...	6.453 0.096	...
	74/ 6/21 14:02	...	-12.113 0.143	...
	74/ 8/ 6 20:50	...	-0.951 0.176	...
DSS63	77/ 1/31 6:34	-23453± 3	4.869±0.143	...
	9:12	-23440 4	5.561 0.388	...
	10:52	-23562 7	4.420 1.58	...
	77/ 4/13 3:03	-41060 6	-2.520 0.180	...
	6:45	-41068 3	-2.752 0.248	3.1 ± 6.3
	78/ 7/31 0:34	-6499 2	-0.020 0.135	...
	3:44	...	0.020 0.105	...
	5:10	-6501 2	...	...
	6:46	...	0.047 0.072	...
	78/ 9/ 4 13:36	...	-1.751 0.221	...
	16:54	-7667 4	...	...
	18:15	...	-1.764 0.134	...
	78/10/30 2:06	-3799 2	0.115 0.035	...
	6:35	-3798 2	0.129 0.031	...
	78/11/ 5 22:28	-3665 1	0.384 0.013	...
	78/11/ 6 9:37	-3662 1	0.312 0.017	...
	79/11/15 22:44	7019 0.1	1.753 0.006	...
	79/11/25 21:46	8043 0.6	0.423 0.015	...
	79/11/26 4:45	8050 0.6	0.354 0.014	...
	12:03	8051 0.8	0.315 0.013	...
	17:01	8049 3.7	0.353 0.061	...
	79/12/21 16:58	8745 1	0.418 0.012	...
	79/12/27 13:10	9302 0.9	0.545 0.007	...
	21:03	9302 0.8	0.589 0.023	...
	79/12/28 2:15	9303 0.8	0.561 0.019	...
	80/ 1/25 21:44	10275 0.9	0.595 0.011	...
	80/ 1/26 9:36	10256 18	0.988 0.391	...
	80/ 2/13 22:17	7649 0.5	-0.098 0.009	...
	80/ 2/14 10:01	7650 0.6	-0.146 0.005	...
	80/ 2/24 13:00	7758 0.8	0.086 0.007	...
OVRO	78/ 2/25 3:36	-11424±0.3	-0.109±0.006	...
	17:28	-11424 0.3	-0.180 0.004	...
	78/ 2/26 5:38	-11428 0.7	-0.092 0.010	...
	15:53	-11420 0.5	-0.188 0.005	...

* All sessions are relative to the DSS14 clock except for the OVRO/HAYST session (relative to HAYST) and the 77/1/21, 77/2/13 11/14/43 sessions (relative to DSS11 for some portions).

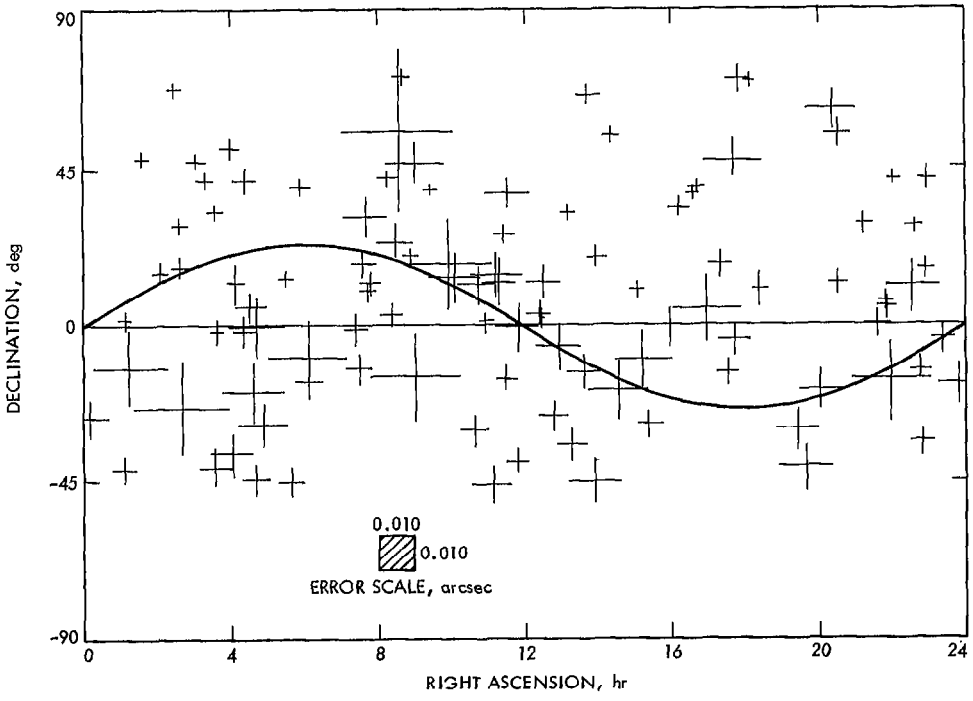

Fig. 1. Source positions and their formal errors from a fit to 1971–80 VLBI data

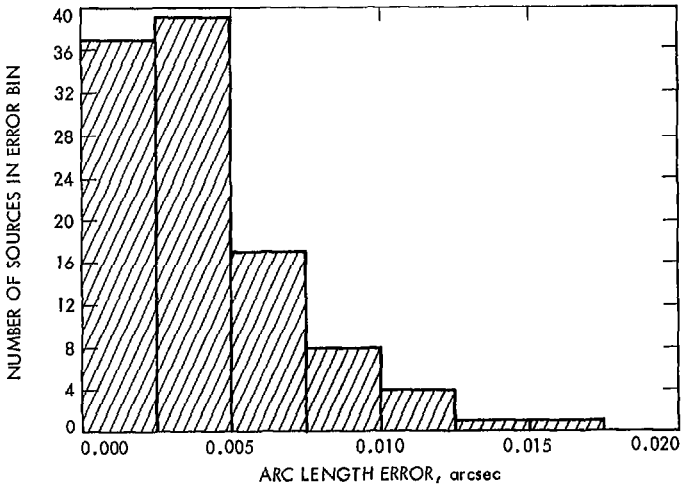

Fig. 2. Histogram of right ascension formal errors in the fit to 1971–80 data

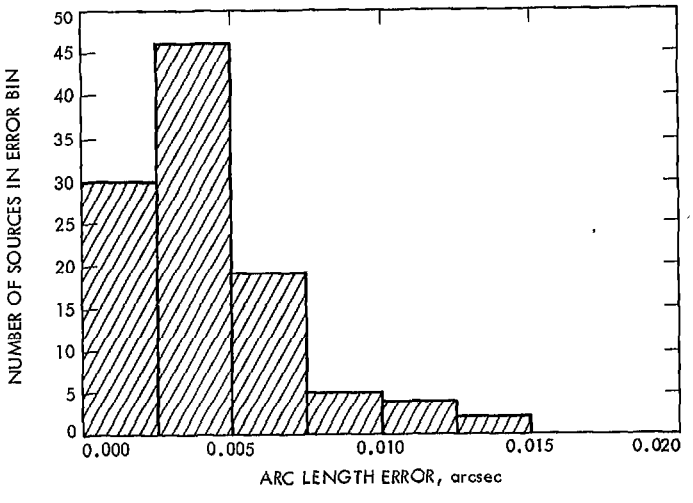

Fig. 3. Histogram of declination formal errors in the fit to 1971–80 data

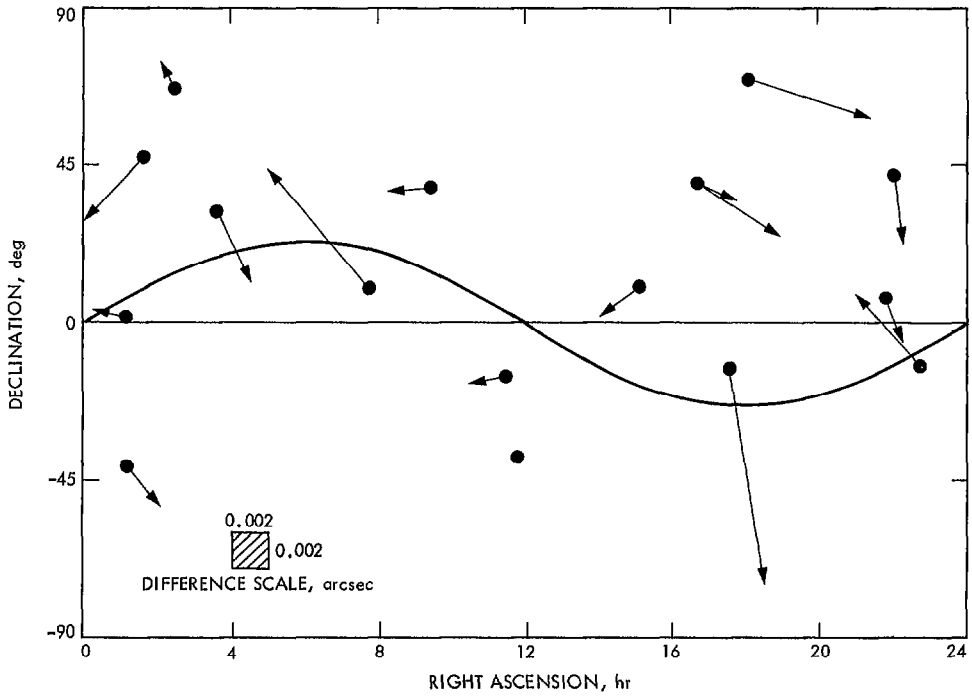

Fig. 4. Source position differences: 1971–78 minus 1979–80 for 17 sources. The difference vector points away from the filled circle specifying the 1979–80 source position. Note the scale change for position and difference.

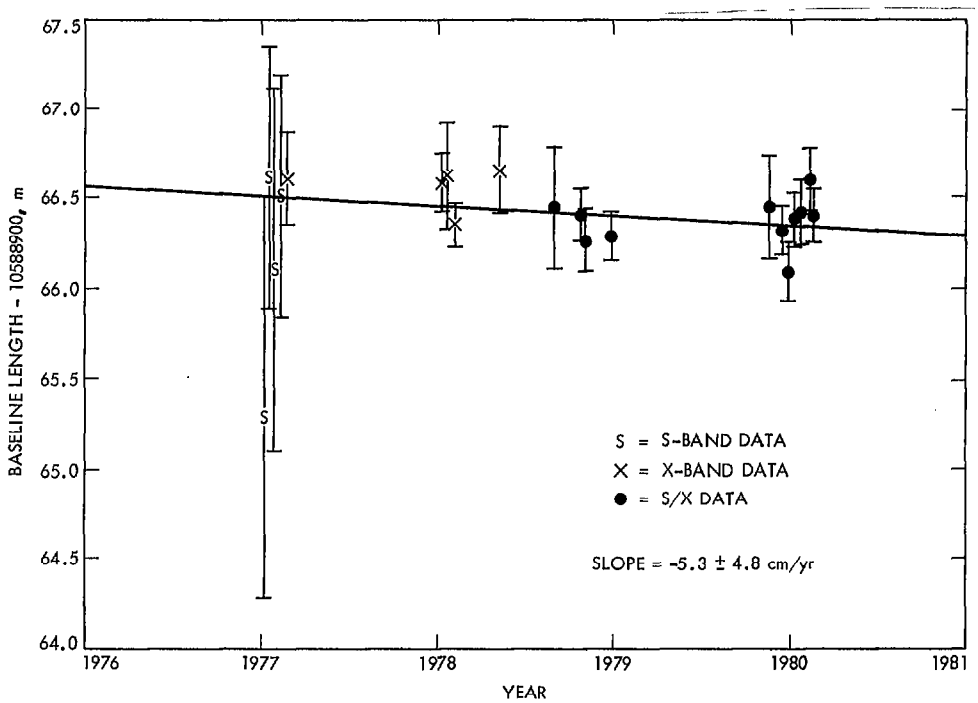

Fig. 5. Length of the California-Australia baseline as a function of time from a fit to 1977–80 VLBI data

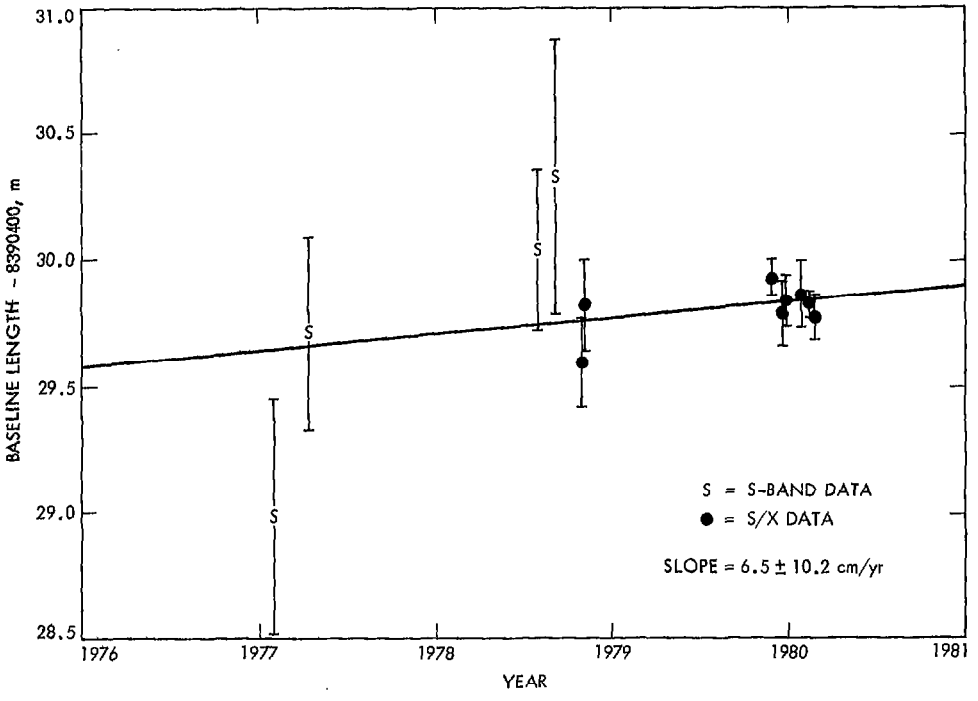

Fig. 6. Length of the California-Spain baseline as a function of time from a fit to 1977–80 VLBI data

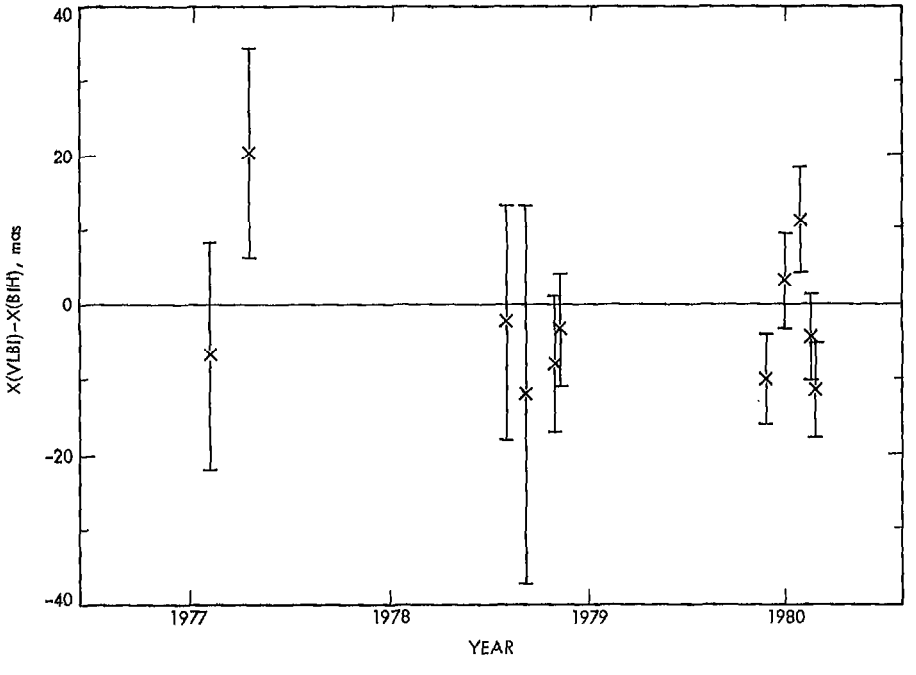

Fig. 7. Polar motion X-component results from 1977–1980 VLBI data

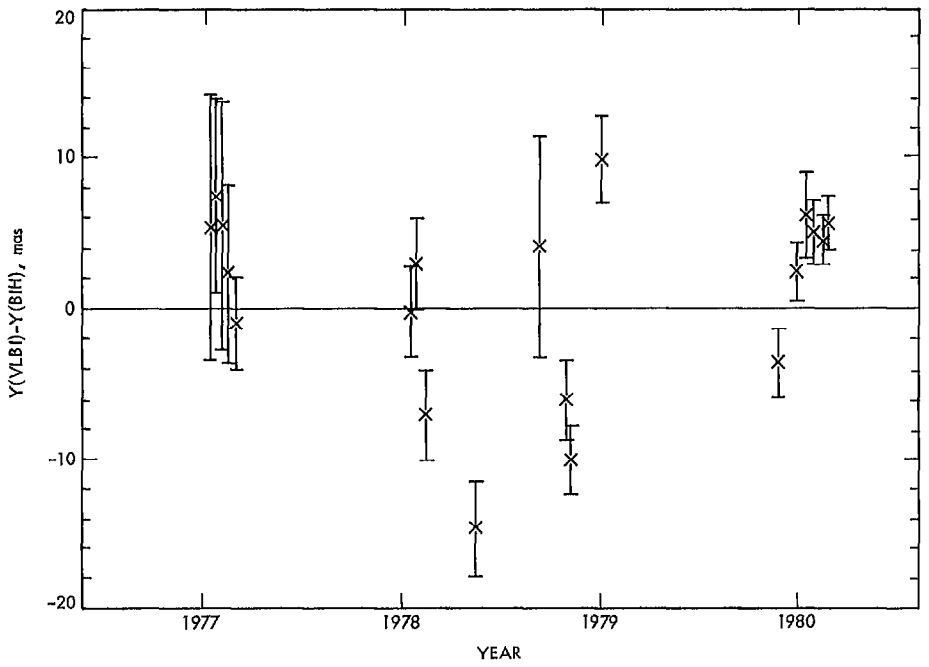

Fig. 8. Polar motion Y-component results from 1977–1980 VLBI data

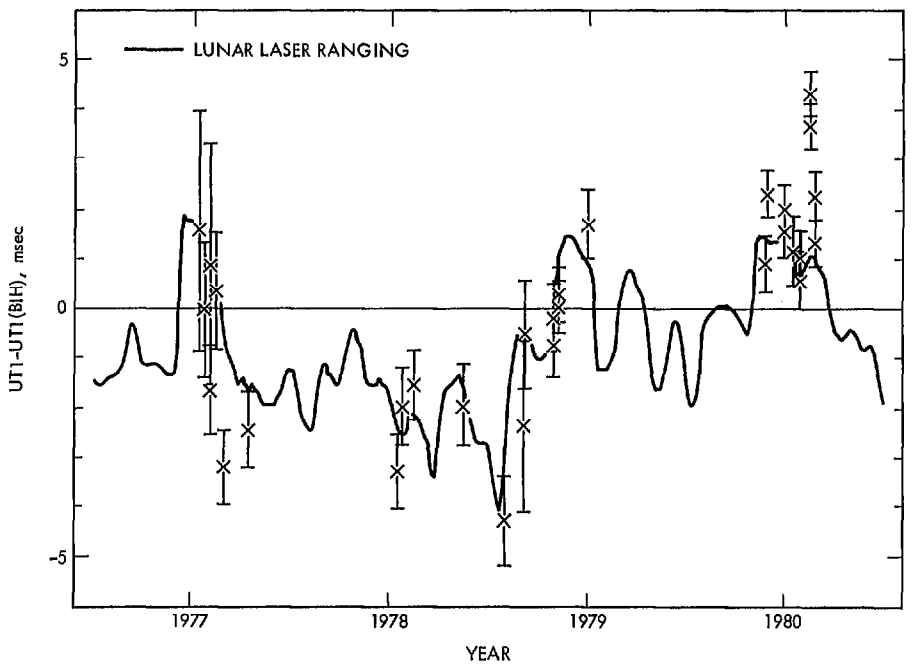

Fig. 9. UT1 results from 1977–1980 VLBI data